

# Second sheet $\sigma$ -pole and the threshold enhancement of the spectral function in the scalar-isoscalar meson-sector

A. Patkós<sup>a</sup> \*, Zs. Szép<sup>a</sup> †, and P. Szépfalussy<sup>b,c</sup> ‡

<sup>a</sup> *Department of Atomic Physics,*

<sup>b</sup> *Department of Physics of Complex Systems,  
Eötvös University, H-1117 Budapest, Hungary*

<sup>c</sup> *Research Institute for Solid State Physics and Optics,  
Hungarian Academy of Sciences, H-1525 Budapest, Hungary*

The scalar-isoscalar propagator of the effective linear  $\sigma$ -model of meson dynamics is investigated with the help of an expansion in the number of the Goldstone-bosons. A generic scenario is suggested for the temperature/density driven evolution of its pole in the second Riemann sheet. An extended temperature range, correlated with characteristic pole locations, is found where the phenomenon of threshold enhancement takes place in the corresponding spectral function.

## I. INTRODUCTION

The aim of the present investigation is to relate the so-called  $\sigma$ -pole in the second Riemann sheet in the complex frequency plane and the behavior of the corresponding spectral function at finite temperature/density. Both objects will be determined from the scalar-isoscalar propagator. The calculation suggests a generic trajectory for this pole irrespective of the nature of the thermodynamical driving force. We investigated the question of when a well-defined resonance characterized by a Lorentzian shaped spectral function is present. The study is performed in the framework of the linear  $\sigma$ -model, used as an effective field theory describing the fluctuations of the chiral order parameter. We find the most convenient the application of an expansion in the number of the Goldstone mesons, which is a kind of large  $N$  approach to the physical excitation spectra of the relativistic  $O(N)$  field theory in its broken symmetry phase.

The application of the  $O(N)$  symmetric scalar field theory to the thermal and finite baryonic density behavior of the pion-sigma system was suggested and has been actively pursued for about 15 years, in particular by Hatsuda, Kunihiro, and collaborators (for the latest review see [1]). The main physical effect proposed for the scalar-isoscalar spectral function is its gradual enhancement near that value of the temperature/baryon density where the phase space available for the  $\sigma \rightarrow 2\pi$  decay is squeezed to zero.

For the theoretical consolidation of this effect, Hatsuda *et al.* put forward apparently model independent arguments for the behavior of both the real and imaginary parts of the  $\sigma$  propagator. Using an improved version of the finite temperature/density perturbative evaluation of the  $\sigma$  self-energy [2] the pole describing the  $\sigma$ -resonance moves from its zero temperature/density location smoothly to the location of the two-pion threshold. Both real and imaginary parts of the pole location diminish monotonically. The real part approaches the two-pion threshold faster than the imaginary part vanishes, and the spectral function becomes proportional in this temperature range to the inverse of the imaginary part [3]. The maximum of the proposed threshold enhancement occurs for that well-defined temperature/density value when the  $\sigma$ -pole reaches the threshold.

The effects of partial symmetry restoration realized by the diminishing of  $f_\pi$  was studied also on the unitarized  $\pi - \pi$  scattering amplitude [4]. This quantity was computed and analyzed recently with dispersive techniques in the framework of the chiral perturbation theory [5].

The approximations made by these authors may be verified soon when reliable spectral functions will be obtained using the non-perturbative lattice field theoretical approach [6, 7]. In the meantime different semi-analytic approximation schemes also might shed light on the generality of the proposed arguments. A possible scheme can be based on an expansion in the inverse number of the Goldstone bosons.

The large  $N$  expansion has been applied already some 30 years ago to the characterization of the elementary excitations of critical  $O(N)$  symmetric lattice systems [8, 9]. It was realized that it provides faithful information on the excitation spectra of these systems in the full broken symmetry phase between zero and the critical temperature.

In a recent letter [10] we proposed its application to the present relativistic system, since it avoids all problems of principles showing up in other perturbative approaches. First of all its validity does not depend on the rather strong self-coupling of the effective  $\sigma$ -model. Second, its result is not sensitive to the choice of the normalization point,

---

\* Electronic address: patkos@ludens.elte.hu

† Present address: Research Group for Statistical Physics of the Hungarian Academy of Sciences, H-1117, Budapest, Hungary. Electronic address: szepzs@antonius.elte.hu

‡ Electronic address: psz@galahad.elte.hu

that is its change can be always compensated by an appropriate change in the value of the couplings as required by the renormalization group. Third, it leads automatically to the same spectra for the elementary  $\sigma$ -field and for the scalar-isoscalar quadratic composite field. In other approaches this feature is usually missing or found to be true after non-trivial manipulations. Finally, in the chiral limit it provides a correct critical description of the chiral symmetry restoration.

The leading order large  $N$  approximation has been applied to the Goldstone boson scattering by Chivukula and Golden [11] at zero temperature. They have explicitly checked that this approximation fulfills in the scalar-isoscalar channel the unitarity condition and also satisfies the Adler-zero condition.

The large  $N$  leading order amplitude  $(N - 1)A(s)$  has been compared also with the existing phase shift data in the  $I = J = 0$  channel of the  $\pi - \pi$  scattering by Dobado and Morales [12]. They have completed the leading order amplitude by subleading terms, dictated by the requirement of crossing symmetry:  $A_{00}(s, t, u) = 3A(s) + A(t) + A(u)$ . Though this is not a systematic next-to-leading order computation the authors found a satisfactory fit to the relevant phase shift  $\delta_0^0(s)$  up to  $\sqrt{s} \approx 600\text{MeV}$ .

To our best knowledge no application of the large  $N$  approach at finite temperature/baryon density was attempted to date. In view of the importance of  $t$ - and  $u$ -channel exchange contributions to the  $\pi - \pi$  scattering amplitude, emphasized in the recent literature [13], a fully satisfactory large  $N$  treatment will also require the calculation of the next-to-leading order contribution to the  $\sigma$  propagator. The leading order calculation presented in this paper is a necessary intermediate step also towards this goal.

The fact that for  $T = 0$  the real and imaginary parts of the  $\sigma$ -resonance are of comparable magnitude implies that for its finite temperature description we cannot restrict ourselves to the immediate vicinity of the real axis. An exception is when the  $\sigma$ -resonance gets close to the two-pion threshold, which is the situation where threshold enhancement develops. For the explanation of the detailed features of this phenomenon it is unavoidable to trace the complete temperature driven pole trajectory. The main purpose of the present paper is to carry out such an investigation within the leading order of the large  $N$  expansion. According to our calculation to be presented in this paper, the  $\sigma$  self-energy continued analytically into the lower halfplane leads to a pole trajectory (when the temperature  $T$  or the baryonic density,  $n_B$  is varied) whose real part assumes smaller values than twice the pion mass, while the decrease of the imaginary part is not drastic. As a consequence of this the pole loses its meaning as a resonance and at the same time in the spectral function the direct neighborhood of the threshold will be emphasized. When further increasing  $T/n_B$  the trajectory hits the real axis on the second Riemann sheet and moves along it before it reaches the threshold. This pole evolution will be demonstrated to be generic in the sense that it is insensitive to the variation of the parameters of the theory. One can argue that it can stay valid beyond the leading order large  $N$  approximation, since it is unlikely that the trajectory would hit the threshold point directly. Only in the limiting chiral symmetric case do we find the smooth behavior which was proposed by Hatsuda *et al.* [1].

One should be aware of the fact that in scalar models a tachyonic pole is always present [14, 15, 16] related to the Landau-ghost phenomenon. It restricts the range of variation of the renormalized parameters where the model can be used in an effective sense at all. For this reason we find in the leading large  $N$  approximation that a parametrization accounting for the  $T = 0$  phenomenological data of the  $\pi$  and  $\sigma$  mesons can be achieved only approximately. However, we shall argue that the relationship between the pole trajectory and the variation of the spectral function to be described below might not change qualitatively.

The presentation of the paper is aimed at a self-contained, technically transparent description. In section II the Schwinger-Dyson equations for the finite temperature two-point functions of the linear  $\sigma$  model are given to leading order in  $N$ . Their analytical continuation onto the second Riemann sheet in the complex frequency variable is presented in section III. Its explicit expression was found by studying the bubble diagram, describing the splitting of the  $\sigma$ -field into two off-shell pions. In section IV we analyze the temperature driven evolution of the  $\sigma$  pole-trajectory. This investigation makes use of the  $T = 0$  parametrization of the model as an input, therefore one first works out the details of the physical and unphysical poles for  $T = 0$ . Here we fix all couplings in a way to achieve the closest possible characteristics of the  $\sigma$  to the particle data, and still staying by a factor of 2 to 3 below the “energy scale” of the tachyon. In the second part of the section we shall argue that the pole-trajectory found by varying the temperature remains qualitatively the same when the system evolves under the variation of the baryonic density. A detailed discussion of the change in the pole trajectory pattern with the pion mass is also presented. The spectral function of  $\sigma$  is computed in section V by approaching the real axis from the physical upper half-plane. We shall analyze also the function which arises when the threshold factor is divided out. It will be demonstrated that in an extended temperature range the maximum of the spectral function is located in the closest neighborhood of the ( $T$ -dependent) position of the two-pion threshold. The extension of this interval is very well correlated with the piece of the pole trajectory, when its real part is below the two-pion threshold. In section VI the conclusions of the present study are summarized.

## II. LEADING LARGE $N$ EXPRESSION OF THE PROPAGATORS AT FINITE TEMPERATURE

The appropriate parametrization of the  $O(N)$  symmetric Lagrangian for a large  $N$  expansion has the following form:

$$L = \frac{1}{2}[\partial_\mu \phi^a \partial^\mu \phi^a - m^2 \phi^a \phi^a] - \frac{\lambda}{24N}(\phi^a)^2(\phi^b)^2 + \sqrt{N}h\phi^1. \quad (1)$$

The last term explicitly breaks the  $O(N)$  symmetry and introduces non-zero mass for pions.

In the broken symmetry phase one separates the expectation value  $\Phi(T)$  of the field, which points along the direction  $a = 1$  in the internal space

$$\phi^a \rightarrow (\sqrt{N}\Phi(T) + \phi^1, \phi^i). \quad (2)$$

In the following all quantities will be computed to leading order in the large  $N$  limit.

The quantum fluctuations of the order parameter are divided into a longitudinal mode, which represents the  $\sigma$  meson and the transversal ones. The latter correspond to the Goldstone modes, the pions. Their mass,  $m_G(T)$  is determined as the pole of the resummed pion propagator, in which the tadpole contribution is calculated with the pion propagator selfconsistently. This results in the following gap equation:

$$m_G^2(T) = m^2 + \frac{\lambda}{6}\Phi^2(T) + \frac{\lambda}{6N}\langle(\phi^a)^2\rangle = m^2 + \frac{\lambda}{6}\Phi^2(T) + \frac{\lambda}{6}\int\frac{d^3k}{(2\pi)^3}\frac{1}{2\omega_k}(1+2n(\omega_k)), \quad (3)$$

where  $n(\omega_k) = 1/(\exp(\omega_k/T) - 1)$  and  $\omega_k = \sqrt{k^2 + m_G^2(T)}$ .

The equation of state obtained from the requirement  $\langle\phi^1\rangle = 0$  is as follows:

$$\sqrt{N}\Phi(T)\left[m^2 + \frac{\lambda}{6}\Phi^2(T) + \frac{\lambda}{6}\int\frac{d^3k}{(2\pi)^3}\frac{1}{2\omega_k}(1+2n(\omega_k)) - \frac{h}{\Phi(T)}\right] = 0. \quad (4)$$

Comparing this with Eq.(3) one can observe that for  $\Phi(T) \neq 0$  consistency requires  $m_G^2(T) = h/\Phi(T)$ . This is precisely the Goldstone theorem in the presence of explicit symmetry breaking.

At leading large  $N$  order the contribution to the longitudinal self energy is given by the sum of the contributions corresponding to the diagrams of Fig.1, i.e. the bubble series. On both internal lines of a bubble exclusively the propagation of pion fields are taken into account to leading order in  $N$ . In each term of the bubble contribution there is a common multiplicative vertex contribution coming from the two edges of each diagram. The bubble series consistently takes into account the non-zero classical value for  $\Phi(T)$ , partly by the implicit dependence of  $m_G^2(T)$ , due to the gap equation and also by the two legs of the effective 4-point vertex formed by the sum of the bubble-series.

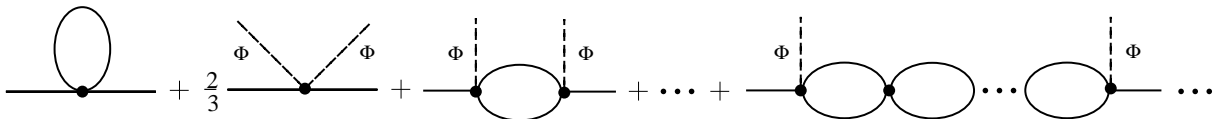


FIG. 1: Diagrams determining the self-energy of the  $\sigma$  field represented to leading order in  $N$ . The external solid lines correspond to the  $\sigma$ , while in the internal bubbles pions propagate. The dashed line represents the expectation value  $\Phi \equiv \Phi(T)$ . The vertices can be read from Eq. (1) after the shift defined in Eq. (2) is performed.

By adding the tree level mass  $m^2$  to the self-energy of the  $\sigma$  field determined in the background  $\Phi(T)$ , using Eq. (4) one finds for the effective  $\sigma$ -mass a simple expression in terms of  $b(p)$ , denoting the value of the single bubble diagram:

$$m_\sigma^2(p) = \frac{h}{\Phi(T)} + \frac{\lambda}{3}\Phi^2(T) \left[ 1 + \frac{\lambda}{6}b(p) + \left(\frac{\lambda}{6}b(p)\right)^2 + \dots \right] = \frac{h}{\Phi(T)} + \frac{\lambda\Phi^2(T)/3}{1 - \lambda b(p)/6}. \quad (5)$$

The bubble contribution with external momentum  $p = (p_0, \mathbf{p})$  is the sum of a zero temperature and a  $T$ -dependent part,  $b^>(p) = b_0^>(p) + b_T^>(p_0, \mathbf{p})$ . The superscript  $>$  hints at the fact that the expression of the bubble contribution is valid in the upper  $p_0$  half-plane. The explicit expressions of the two terms read as follows:

$$b_0^>(p) = i \int \frac{d^4k}{(2\pi)^4} \frac{1}{k^2 - m_G^2(T) + i\epsilon} \frac{1}{(p+k)^2 - m_G^2(T) + i\epsilon}, \quad (6)$$

$$b_T^>(p) = \int \frac{d^3\mathbf{q}}{(2\pi)^3} \frac{1}{4\omega_1\omega_2} \left\{ (n_1 + n_2) \left[ \frac{1}{p_0 - \omega_1 - \omega_2 + i\epsilon} - \frac{1}{p_0 + \omega_1 + \omega_2 + i\epsilon} \right] - (n_1 - n_2) \left[ \frac{1}{p_0 - \omega_1 + \omega_2 + i\epsilon} - \frac{1}{p_0 + \omega_1 - \omega_2 + i\epsilon} \right] \right\}, \quad (7)$$

where  $n_i = 1/(\exp(\beta\omega_i) - 1)$  and  $\omega_1 = (\mathbf{q}^2 + m_G^2(T))^{1/2}$ ,  $\omega_2 = ((\mathbf{q} + \mathbf{p})^2 + m_G^2(T))^{1/2}$ , and  $\epsilon > 0$ .

Using cut-off regularization the zero temperature bubble contribution is:

$$b_0^>(p) = \frac{1}{16\pi^2} \left[ \ln \frac{m_G^2(T)}{\Lambda^2} - 1 - \sqrt{1 - \frac{4m_G^2(T)}{p^2}} \left( \ln \frac{1 - \sqrt{1 - 4m_G^2(T)/p^2}}{1 + \sqrt{1 - 4m_G^2(T)/p^2}} + i\pi \right) \right]. \quad (8)$$

It is common to discuss the spectral function for  $\mathbf{p} = 0$ , when the expression of the finite temperature bubble contribution simplifies to:

$$b_T^>(p_0) = -\frac{1}{4\pi^2} \int_{m_G(T)}^{\infty} \frac{dq_0}{q_0} \sqrt{q_0^2 - m_G^2(T)} \left[ \frac{n(q_0)}{2q_0 - p_0} + \frac{n(q_0)}{2q_0 + p_0} \right], \quad \text{Im } p_0 > 0. \quad (9)$$

In view of the quadratic and logarithmic cut-off dependencies which appear in Eqs.(3),(4) and (8) a mass- and coupling constant renormalization is necessary. It requires the introduction of a normalization scale  $M_0$ . This scale should lie below the scale of the tachyonic pole to be discussed below. Its choice within the relevant range where the  $O(N)$  model can serve for the effective description of hadron dynamics should not affect sensitively the physical results.

The expressions of the renormalized couplings go beyond the accuracy of the usual one-loop relations. Actually, they ensure that a change in the normalization scale can be compensated in all formulae below by an appropriate change in the couplings. The following non-perturbative mass- and self-coupling renormalizations are introduced:

$$\frac{m^2}{\lambda} + \frac{\Lambda^2}{96\pi^2} = \frac{m_R^2}{\lambda_R}, \quad \frac{1}{\lambda} + \frac{1}{96\pi^2} \ln \frac{e\Lambda^2}{M_0^2} = \frac{1}{\lambda_R}. \quad (10)$$

In terms of the renormalized couplings the equation of state Eq.(4) can be cast into the following explicitly finite form:

$$\begin{aligned} & \frac{\lambda_R}{6} \frac{\Phi_0^2}{m_{G_0}^2} \left( \frac{m_{G_0}^4}{m_G^4(T)} - 1 \right) + \frac{\lambda_R}{96\pi^2} \left[ \left( \frac{m_G^2(T)}{m_{G_0}^2} - 1 \right) \ln \frac{m_{G_0}^2 e}{M_0^2} + \frac{m_G^2(T)}{m_{G_0}^2} \ln \frac{m_G^2(T)}{m_{G_0}^2} \right] \\ & + \frac{\lambda_R T^2}{12\pi^2 m_{G_0}^2} \int_{m_G(T)/T}^{\infty} dy \frac{\sqrt{y^2 - m_G^2(T)/T^2}}{\exp(y) - 1} = \frac{m_G^2(T)}{m_{G_0}^2} - 1. \end{aligned} \quad (11)$$

Here  $m_{G_0}$  and  $\Phi_0$  stand for the  $T = 0$  value of the Goldstone mass and of the expectation value of the  $\sigma$  field, respectively.

The formal expression of the effective mass term of the  $\sigma$ -propagator (5) is unchanged after renormalization, just  $\lambda_R$  should replace  $\lambda$  and for the  $T = 0$  contribution of  $b(p)$  in Eq. (8) the scale  $M_0^2$  is put in place of  $e\Lambda^2$ .

The finite part of the zero temperature bubble contribution defined in this way has different forms depending on the range of  $p_0$  values:

$$b_0^>(p_0) = \frac{1}{16\pi^2} \begin{cases} \left[ \ln \frac{m_G^2(T)}{M_0^2} + 2\sqrt{\frac{4m_G^2(T)}{p_0^2} - 1} \times \arctan \left( \frac{4m_G^2(T)}{p_0^2} - 1 \right)^{-\frac{1}{2}} \right], & p_0 < 2m_G(T) \\ \left[ \ln \frac{m_G^2(T)}{M_0^2} - \sqrt{1 - \frac{4m_G^2(T)}{p_0^2}} \left( \ln \frac{1 - \sqrt{1 - 4m_G^2(T)/p_0^2}}{1 + \sqrt{1 - 4m_G^2(T)/p_0^2}} + i\pi \right) \right], & p_0 > 2m_G(T). \end{cases} \quad (12)$$

### III. ANALYTICAL CONTINUATION OF THE PROPAGATORS ONTO THE SECOND RIEMANN SHEET

The interpretation of the temperature driven variation of the spectral function will be based on the study of the variation of the scalar-isoscalar pole mass, that is the zero of  $G_\sigma^{-1}(p_0, \mathbf{p} = 0) = p_0^2 - m_\sigma^2$  in the lower  $p_0$  halfplane. For this it is necessary to construct an analytical continuation of the longitudinal propagator onto the second Riemann sheet. By Eq.(5) it is clear that the problem is equivalent to the continuation of  $b(p_0)$ , which will be discussed in this section.

We decided to perform the analytical continuation in such a way that  $b(p_0)$  varies continuously when the real axis is crossed above the two-pion threshold  $p_0 > 2m_G(T)$ . This implies that the bubble contribution is discontinuous across the real axis for  $-2m_G(T) < p_0 < 2m_G(T)$ . We will actually see that there it is  $\text{Re } b(p_0)$  which is discontinuous.

Above the threshold on the real axis both the real and imaginary parts of the zero temperature bubble are continuous as one can see from the second line of Eq. (12). In view of this, for values of  $p_0$  below the real axis (lying on the second

Riemann sheet) we simply use the expression written in the second line of Eq. (12). We denote this continuation  $b_0^<(p_0)$ . (In this sense the indices “>” and “<” on  $b_0$  are redundant, yet we keep them for the sake of clarity.)

We turn now to the finite temperature part of the bubble. For real values of  $p_0$ , above the threshold the real part of  $b_T(p_0)$  can be obtained by taking the principal value in the right hand side of Eq. (9):

$$\text{Re } b_T^>(p_0) = \frac{1}{4\pi^2} \mathcal{P} \int_{m_G(T)/T}^{\infty} dx \frac{\sqrt{x^2 - m_G^2(T)/T^2}}{p_0^2/4T^2 - x^2} \frac{1}{\exp(x) - 1}. \quad (13)$$

Introducing the parametrization  $p_0 = \text{Re}p_0 + i\varepsilon$  we can evaluate the imaginary part of  $b_T(p_0)$  in the neighborhood of the real axis both for  $\varepsilon > 0$  (the physical prescription) and for  $\varepsilon < 0$ :

$$\begin{aligned} \text{Im} \int_{m_G(T)}^{\infty} \frac{dq_0}{q_0} \sqrt{q_0^2 - m_G^2(T)} \frac{n(q_0)}{2q_0 \pm (\text{Re}p_0 + i\varepsilon)} \\ = -\pi \int_{m_G(T)}^{\infty} \frac{dq_0}{q_0} \sqrt{q_0^2 - m_G^2(T)} n(q_0) \delta(2q_0 - |\text{Re}p_0|) (\Theta(\pm\varepsilon) - \Theta(\mp\varepsilon)). \end{aligned} \quad (14)$$

With this one obtains:

$$\text{Im} b_T(p_0) = -\frac{\text{sgn}(\varepsilon)}{8\pi} \frac{\sqrt{(\text{Re}p_0)^2 - 4m_G^2(T)}}{\text{Re}p_0} n(|\text{Re}p_0|/2) \left[ \Theta(\text{Re}p_0 - 2m_G(T)) + \Theta(-\text{Re}p_0 - 2m_G(T)) \right]. \quad (15)$$

In order to ensure the continuity of the imaginary parts an extra term has to be added to the expression used in the upper half-plane for the bubble:

$$b_T^<(p_0) = b_T^>(p_0) - \frac{i}{4\pi} n(p_0/2) \sqrt{1 - \frac{4m_G^2(T)}{p_0^2}}. \quad (16)$$

For later use (among others for the computation of the spectral function) it is useful to write explicit expressions for the physical values of  $b(p_0)$  on the real positive axis. We have  $b_T^>(p_0) = \text{Re } b_T^>(p_0) + i \text{Im } b_T^>(p_0)$ , where the first term is given by Eq.(13), and

$$\text{Im } b_T^>(p_0) = -\frac{1}{8\pi} \sqrt{1 - \frac{4m_G^2(T)}{p_0^2}} n(p_0/2) \Theta(p_0 - 2m_G(T)). \quad (17)$$

The bubble is fully real below the threshold and it is clear that the integral in Eq. (13) is not singular for  $p_0 < 2m_G(T)$ . Its integrand has for  $p_0 = 2m_G(T)$  an integrable square root singularity:

$$\text{Re } b_T^>(p_0 = 2m_G(T)) = -\frac{1}{4\pi^2} \int_{m_G(T)/T}^{\infty} dx \frac{1}{\sqrt{x^2 - m_G^2(T)/T^2}} \frac{1}{\exp(x) - 1}.$$

For complex  $p_0$  also in the lower halfplane one can use for  $b_0^<(p_0)$  the expression written on the second line of Eq. (12) and the complete expression of  $b_T^<(p_0)$  reads as

$$b_T^<(p_0) = \frac{1}{4\pi^2} \int_{m_G(T)/T}^{\infty} dx \frac{\sqrt{x^2 - m_G^2(T)/T^2}}{p_0^2/4T^2 - x^2} \frac{1}{\exp(x) - 1} - \frac{i}{4\pi} n(p_0/2) \sqrt{1 - \frac{4m_G^2(T)}{p_0^2}}. \quad (18)$$

#### IV. THE TEMPERATURE DEPENDENCE OF THE $\sigma$ -POLE

In this section the temperature driven variation of the pole of  $G_\sigma(p_0)$ , located in the fourth quadrant of the complex  $p_0$  plane will be found. We shall argue that the generic scenario of its variation is realized independently of what thermodynamical quantity would drive this variation. As an illustration of this we shall discuss the pole trajectory under the change of the baryonic charge density implemented following Hatsuda, Kunihiro, and Shimizu [3].

For the solution of the equation

$$G_\sigma^{-1}(p_0) \left( 1 - \frac{\lambda_R}{6} b^<(p_0) \right) = (p_0^2 - m_G^2(T)) \left( 1 - \frac{\lambda_R}{6} (b_0^<(p_0) + b_T^<(p_0)) \right) - \frac{\lambda_R}{3} \Phi^2(T) = 0 \quad (19)$$

one obviously should know  $\Phi(T)$  (and  $m_G^2(T) = h/\Phi(T)$ ), calculable from the renormalized equation of state (11). This equation requires two inputs. The phenomenological (physical) input is  $\Phi_0^2/m_{G_0}^2 = \Phi_0^3/h \equiv f_\pi^2/4m_{G_0}^2 \sim 0.11$ , but in the equation of state also the normalization scale appears explicitly.

In order to simplify the formulae we have decided to choose the absolute value of the pole location at  $T = 0$  for the normalization scale  $M_0$ . Therefore one has to find first the  $\sigma$ -pole for this temperature and only then one can turn to the discussion of the finite temperature variation.

### A. The poles of $G_\sigma(p_0)$ at $T = 0$

We parametrize the solution of the equation

$$G_\sigma^{-1}(p_0) \left(1 - \frac{\lambda_R}{6} b_0^<(p_0)\right) = (p_0^2 - m_{G_0}^2) \left(1 - \frac{\lambda_R}{6} b_0^<(p_0)\right) - \frac{\lambda_R}{3} \Phi_0^2 = 0 \quad (20)$$

in the form  $p_0 = M_0 \exp(-i\varphi_0)$ ,  $0 < \varphi_0 < \pi/2$ . Note, that the renormalization scale is fixed in proportion to  $m_{G_0}$  once a renormalized coupling is chosen.

One can introduce instead of  $M_0$  and  $\varphi_0$  a more convenient parametrization  $p_0 = 2m_{G_0} + \bar{M}_0 \exp(-i\bar{\varphi}_0)$ , where  $\bar{M}_0$  and  $\bar{\varphi}_0$  are uniquely determined by  $M_0$  and  $\varphi_0$ . Attention has to be payed when switching from one parametrization to the other because changing the scale  $M_0$  means changing the renormalized coupling constant  $\lambda_R$ .

In addition one has to deal with care when realizing numerically the analytic continuation. For the square root and for the evaluation of the argument of the complex numbers appearing in  $b_0^<(p)$  one has to choose a phase convention which ensures the continuous variation of the complex phase of the final complex number with  $\varphi_0$ . Good guidance for how to define the argument of complex numbers in the process of evaluating complicated multivalued functions is provided by their series expansion near the positive real axis above the threshold.

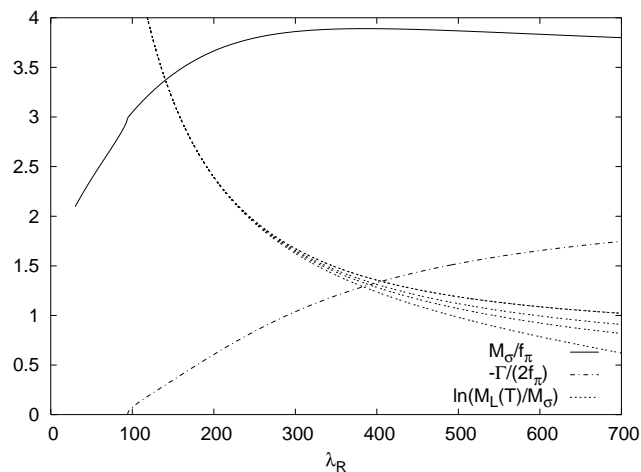


FIG. 2: The real and imaginary parts of the physical poles at  $T = 0$ . Also shown is the logarithm of the tachyon pole position in proportion to the mass of  $\sigma$  for various temperatures. The lines appear in the same order downward from above on the right side of the figure as the labels in the key.

The output is  $M_0/\Phi_0$  and  $\varphi_0$  in terms of which we obtain the mass  $M_\sigma = M_0 \cos \varphi_0$  and the width  $\Gamma = 2M_0 \sin \varphi_0$  of the  $\sigma$  as the real and imaginary parts of the pole. These are shown as a function of the renormalized coupling  $\lambda_R$  in Fig.2. At  $\lambda_R = 400$  one finds the ratio  $M_\sigma/\Gamma \sim 1.4$  with  $M_\sigma = 3.95f_\pi$ . These values are away from the phenomenological expectations [17, 18], but these are the best values we can reach in the leading large  $N$  approximation. The use of higher values of  $\lambda_R$  which appear to be closer to the observed numbers might not be advisable since the a tachyonic pole described below comes very close to the scale  $M_0$  for that coupling region. We will use  $\lambda_R = 400$  henceforth in the finite temperature calculations.

Scalar theories are known to have a tachyonic pole related to the Landau-ghost [16], that is a zero of the inverse propagator on the positive imaginary axis  $p_0 = iM_L$ . Equation (20) takes the following form when looking for  $M_L$ :

$$(M_L^2 + m_{G_0}^2) \left(1 - \frac{\lambda_R}{6} b_0^>(iM_L)\right) + \frac{\lambda_R}{3} \Phi_0^2 = 0. \quad (21)$$

with a fully real expression for  $b_0^>(iM_L)$ :

$$b_0^>(iM_L) = \frac{1}{16\pi^2} \left[ \ln \frac{m_{G_0}^2}{M_0^2} - \sqrt{1 + \frac{4m_{G_0}^2}{M_L^2}} \ln \frac{\sqrt{1 + 4m_{G_0}^2/M_L^2} - 1}{\sqrt{1 + 4m_{G_0}^2/M_L^2} + 1} \right]. \quad (22)$$

With a suitable parametrization, for example,  $M_L/M_0 = \exp(z)$ , one can solve Eq.(21) for  $z$  at a given value of  $\Phi_0^2/m_{G_0}^2$  and using the value of  $M_0/\Phi_0$  obtained by solving Eq.(20). The logarithm of the ratio  $M_L/M_\sigma$  whose value restricts the range of validity of the theory is shown in Fig.2 as a function of  $\lambda_R$ , not only for  $T = 0$  but also for some non-zero temperatures.

## B. Finite $T/n_B$ behavior of the $\sigma$ -pole

The features of the numerical solution of Eq.(19) will be discussed in the main part of the present subsection. It will be pointed out that when moving on the second Riemann sheet its root approaches and eventually hits at a certain temperature the unphysical real axis *below* the two-pion threshold. For the determination of the poles on this piece of the real axis one can evaluate the analytic functions directly. The real solution provides a useful check of the solution based on the complex equation. We give here the corresponding formulae explicitly.

In both parametrizations of the pole one has on the real axis below the threshold ( $p_0 < 2m_G(T)$ ),  $\varphi = \pi, \bar{\varphi} = \pi$ , respectively. Then one has  $(1 - 4m_G^2(T)/p_0^2)^{1/2} = -i(4m_G^2(T)/p_0^2 - 1)^{1/2} \equiv -iQ$ . Using this in Eq. (12) one obtains:

$$\begin{aligned} -\sqrt{1 - \frac{4m_G^2(T)}{p_0^2}} \left( \ln \frac{1 - \sqrt{1 - 4m_G^2(T)/p_0^2}}{1 + \sqrt{1 - 4m_G^2(T)/p_0^2}} + i\pi \right) &= iQ \left( \ln \frac{Q^{-1} + i}{Q^{-1} - i} + i\pi \right) \\ &= -2Q \operatorname{arccot}(Q^{-1}) - \pi Q = 2Q(\operatorname{arccot}(Q) + \pi). \end{aligned} \quad (23)$$

So, on the real axis of the second Riemann sheet, below the threshold one has:

$$b_0^{<-}(p_0) = \frac{1}{16\pi^2} \left[ \ln \frac{m_G^2(T)}{M_0^2} + 2\sqrt{\frac{4m_G^2(T)}{p_0^2} - 1} \left( \arctan \left( \frac{4m_G^2(T)}{p_0^2} - 1 \right)^{-\frac{1}{2}} - \pi \right) \right], \quad (24)$$

$$b_T^{<-}(p_0) = -\frac{1}{4\pi} \sqrt{\frac{4m_G^2(T)}{p_0^2} - 1} \frac{1}{\exp(p_0/2T) - 1} + \frac{1}{4\pi^2} \int_{m_G(T)/T}^{\infty} dx \frac{\sqrt{x^2 - m_G^2(T)/T^2}}{(p_0^2/4T^2 - x^2)} \frac{1}{\exp(x) - 1}. \quad (25)$$

(Here we use a somewhat redundant superscript “-” on  $b^{<}(p)$  in order to emphasize that the formulae refer to a continuation below the threshold).

The evaluation of  $b^{>}(p_0)$  below threshold on the real axis becomes relevant for temperatures when the pole “climbs up” from the second onto the first Riemann sheet and represents a stable  $\sigma$  particle. When approaching this portion of the real axis from the physical upper halfplane one trivially finds the corresponding real expression. For real  $p_0$  the equations which determine the poles on the physical and unphysical real axes below the threshold ( $p_0 < 2m_G(T)$ ) are the following:

$$(p_0^2 - m_G^2(T)) \left( 1 - \frac{\lambda_R}{6} (b_0^{>}(p_0) + b_T^{>}(p_0)) \right) - \frac{\lambda_R}{3} \Phi^2(T) = 0 \quad (26)$$

and

$$(p_0^2 - m_G^2(T)) \left( 1 - \frac{\lambda_R}{6} (b_0^{<-}(p_0) + b_T^{<-}(p_0)) \right) - \frac{\lambda_R}{3} \Phi^2(T) = 0, \quad (27)$$

respectively.

In Fig.3 the trajectory of the real part of the pole position is shown as it evolves with the temperature. In the same figure also the  $T$ -dependent location of the two-pion threshold appears. One notes that  $\operatorname{Re}(p_0)$  crosses below the actual position of the threshold for  $T^{**}/m_{G0} \sim 0.68$ . As it is seen from Fig.3  $\operatorname{Im}(p_0)$  hardly diminishes until this temperature is reached, therefore the relative broadening of  $\sigma$  actually increases. Similar conclusions were drawn in the context of chiral perturbation theory in [19]. Above  $T^{**}$  the imaginary part decreases faster and the pole position is landing on the real axis for  $T_{real}/m_{G0} \sim 0.93$ .

One can study the solutions of Eq.(19) also in the upper  $p_0$  halfplane on the *second* Riemann sheet. One finds that starting from  $T = 0$ , there exists a “mirror”-root, which arrives at the same point of the real axis for  $T = T_{real}$ . This collision of the poles results in two oppositely moving real solutions for higher temperatures. The solutions of Eq.(27) fully confirm this scenario.

The pole moving upwards catches up with the threshold for  $T^*/m_{G0} = 1.074$ . (The other pole first moves downwards, later its motion changes direction, but it lags behind the position of the threshold in the whole temperature range of interest, see. Fig. 3.) It does not stop there, but moves further with increasing temperature, now on the real axis of the physical Riemann sheet. This part of the scenario is confirmed also by the direct solution of Eqs.(27) and (26). The  $T$ -dependent position of the stable physical  $\sigma$  particle is also displayed in Fig.3. One has to notice that all scales increase with the temperature, therefore the tachyon pole puts a strict temperature limit to the validity of the proposed effective treatment of the pion-sigma system.

The scenario obtained is clearly different from the one suggested by Hatsuda, Kunihiro, and their collaborators [1]. In their various approximate descriptions the real part of the pole position never goes below the two-pion threshold until it has a finite imaginary part. In order to test the generic nature of the pole evolution found above, we have followed the procedure proposed by Hatsuda *et al.* [3] for the introduction of finite baryonic charge density  $n_B$  into the

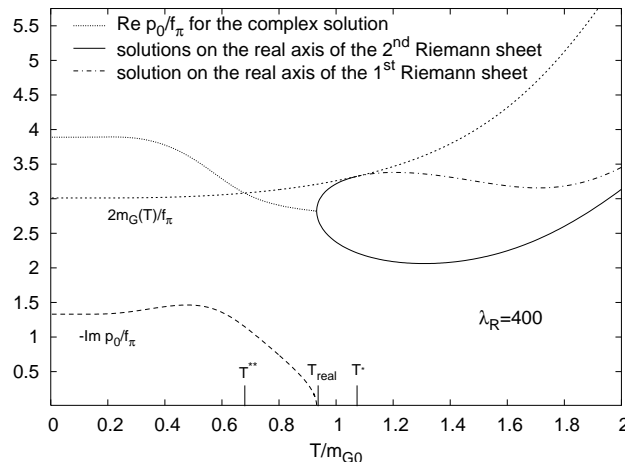


FIG. 3: The temperature dependence of the real and imaginary parts of the  $\sigma$ -pole

effective pion-sigma dynamics. In summary, the nonzero value of  $n_B$  results in a rescaling of the vacuum expectation value  $\Phi$  [20]. At  $T = 0$ , for low densities they propose

$$\Phi(n_B) = (1 - Cn_B)\Phi_0, \quad (28)$$

with  $C = 0.2 - 0.3$ . With the parametrization  $p_0 = \eta M_0 \exp(-i\varphi)$  we have solved Eq.(20) for  $\eta$  and  $\varphi$  with  $\Phi(n_B)$  replacing  $\Phi_0$  everywhere. This equation is much simpler, since the details of its continuation onto the second Riemann sheet are self-evident. Still, we find qualitatively the same pattern for the pole trajectory as one can see in Fig.4. In another test the strength of the explicit symmetry breaking ( $h$ ) was gradually decreased. The distance of the point where the complex solution arrives to the real axis from the two-pion threshold monotonically decreases with the decrease of  $h$ . In the chiral limit it approaches smoothly the origin as it should for a true phase transition. It is worthwhile to point out that the most recent dispersive investigation of Yokokawa *et al.*[5] investigates exactly this limit. They find the same smooth behavior, therefore there is no conflict between the results of the two approaches yet. It will be interesting to see the effect of explicit symmetry breaking in their approach.

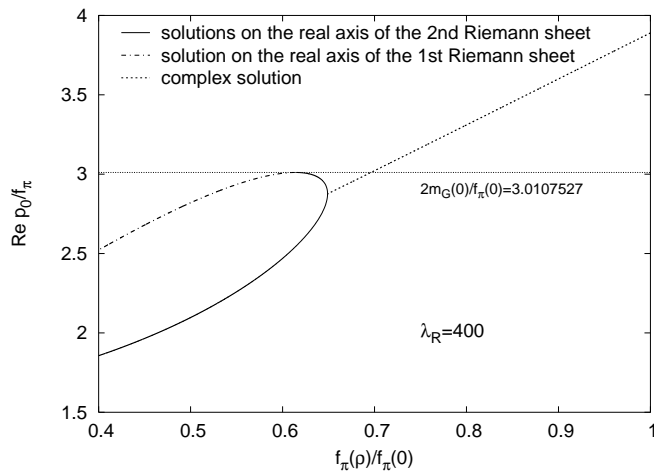


FIG. 4: The dependence of the real part of the pole position on the variation of  $f_\pi$  due to non-zero baryonic density

Finally, we have studied systematically the deformation of the  $T$ -driven pole trajectory when  $2m_{G0}/f_\pi$  is decreased gradually with  $f_\pi$  kept constant. A quite interesting pattern appears in Fig.5. The trajectory reaches closer to the negative imaginary axis as the strength of the explicit symmetry breaking diminishes, before it turns to the real axis, and eventually ends at the two-pion threshold. At some value  $1.317 > 2m_{G0,imag}/f_\pi > 1.316$  it touches first this axis, but is “reflected” from it back into the fourth quarter. For higher temperatures it will have again a non-zero real part.

In order to understand what happens, it is convenient to search directly for poles on the negative imaginary axis. It turns out that already for  $2m_{G0}/f_\pi = 3.01$  one has an infinite number of approximately equidistantly located poles along this axis for finite temperature. Below we call the pole located the closest to the origin the  $\sigma^*$ -pole. Already at low temperature the distance of all these poles from the threshold is much larger, than that of the  $\sigma$ -pole. This



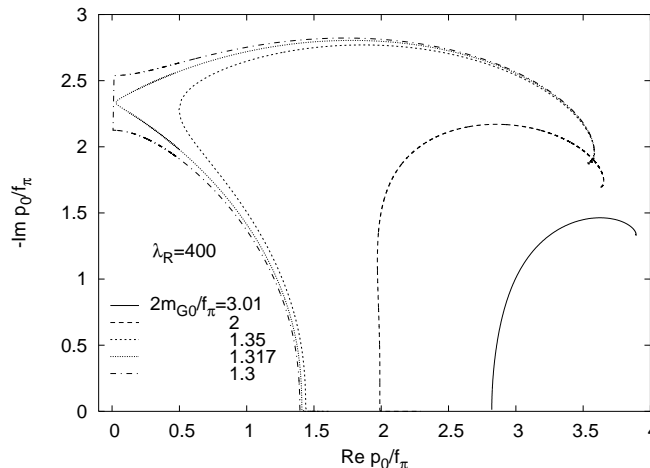


FIG. 5: Trajectory of the complex  $\sigma$ -pole for various values of  $2m_{G0}/f_\pi$ . Note the tendency of the trajectory to approach closer to the imaginary axis as  $m_{G0}$  decreases.

explains why the latter dominates near  $T = 0$  the behavior of the spectral function, as will be argued in the next section. The distance further increases with the increase of the temperature.

It turns out that for the above quoted value of  $2m_{G0,imag}/f_\pi$  the  $\sigma$ -pole and its mirror from the third quarter touch the imaginary axis exactly at the location of the highest (negative) imaginary  $\sigma^*$ -pole at that temperature. The result of the “ $\sigma - \sigma^*$ ” collision is the reflection of the two complex poles back into their respective quarters.

Further decreasing  $2m_{G0}/f_\pi$  the pair of mirror poles arrives onto the negative imaginary axis below the highest imaginary pole. (In Fig. 5 it is above  $\sigma^*$ , since the negative imaginary axis is directed upwards.) The colliding poles now give rise to a purely imaginary pair, one member of which moves towards the origin the other one moving the opposite direction. The pole moving towards the origin collides at some higher temperature with the oppositely moving genuinely imaginary  $\sigma^*$ -pole, and they are pushed back into the complex quarters as mirror poles. Eventually, the pole in the fourth quarter will land on the real axis and moves up to the threshold for  $T^*(m_{G0})$ , where it is converted into a stable particle pole on the physical sheet, as described earlier in this section. In view of the multiple pole collisions it is clear that the stable high- $T$   $\sigma$  particle is not directly related to the  $T = 0$  complex  $\sigma$ -pole.

In the chiral limit the  $\sigma$ -pole reaches the origin and describes the phase transition restoring the chiral symmetry of the model. This simple trajectory has been already discussed in our previous publication [10]. The presence of explicit symmetry breaking with realistic strength led to a rather spectacular change in this scenario. It is a valid question whether a smooth continuous deformation of the pole trajectory connects the case of the explicit symmetry breaking with the chiral limit.

In the region, when the pion mass is much smaller than the temperature for which the complex pole becomes purely imaginary, one can find analytically the first  $\sigma^*$ -pole in the infinite sequence described above. Its location is given approximately as  $p_{\sigma^*}^2 \sim m_G^3(T)T/\Phi^2(T)$ . In view of the fact that  $T/\Phi(T) \sim \mathcal{O}(1)$ , this pole goes faster to zero than the pion mass. Our numerical study shows that the point where the pole lands on the negative imaginary axis does not change more than 10% between the pion mass  $m_{G0,imag}$  and the chiral limit. Therefore the interval of temperatures for which the pole moves on the imaginary axis increases with decreasing pion mass (see Fig.5). Eventually for  $m_{G0} = 0$  the highest negative imaginary pole stays (with zero residuum) in the origin and the scenario characterizing the chiral limit sets in smoothly.

For symmetry breaking much smaller than the parameter characterizing the onset of the dynamical scaling in the chirally symmetric case one can even experience the realization of the scaling behavior.

To some extent the above complicated trajectory is to be expected, since it is highly “improbable” that the roots of a complex equation would move smoothly to a specific point (e.g., the two-pion threshold) of the real axis, irrespective of the variation of its parameters. The limitations of the true resonance interpretation of the  $\sigma$ -pole will be discussed in the next section, when the correlation of its location with the measurable spectral function  $\rho_\sigma$  will be discussed.

## V. THE $T$ DEPENDENCE OF THE SPECTRAL FUNCTION $\rho_\sigma$

The spectral function of the order parameter field  $\sigma$  is defined using the expression of the propagator in the physical half-plane as:

$$\rho_\sigma(p_0, \mathbf{p}, T) = -\frac{1}{\pi} \lim_{\varepsilon \rightarrow +0} \text{Im} G_\sigma(p_0 + i\varepsilon, \mathbf{p}, T). \quad (29)$$

The leading order large  $N$  expression of spectral function, at  $\mathbf{p} = 0$ , is given by

$$\rho_\sigma(p_0, 0, T) = \lambda_R^2 \Phi^2(T) \text{Im}b^>(p_0) / 18\pi \times \left[ \left[ (p_0^2 - m_G^2(T)) \left( 1 - \frac{\lambda_R}{6} \text{Re}b^>(p_0) \right) - \frac{\lambda_R}{3} \Phi^2(T) \right]^2 + (p_0^2 - m_G^2(T))^2 \frac{\lambda_R^2}{36} (\text{Im}b^>(p_0))^2 \right]^{-1}. \quad (30)$$

We have seen that  $\text{Im}b^>(p_0) \neq 0$  only for  $p_0 > 2m_G(T)$ , if there is no stable particle pole below the threshold. Therefore the spectral function is nonzero only for  $p_0$  values above the threshold until  $T < T^*$ . For this reason the numerator and the second term in the denominator of Eq.(30), that is  $\text{Im}b^>(p_0)$  goes to zero when  $p_0 \rightarrow 2m_G(T) + 0$ .

The scalar-isoscalar spectral function is displayed in Fig.6. One notices the shift of its maximum towards the two-pion threshold with increasing temperature, though its width does not decrease initially. For  $T > T^{**}$  the shape of  $\rho_\sigma$  becomes cuspid. Finally, a very high value of the maximum is experienced numerically around  $T/m_{G0} \sim 1.07$ . Above this temperature the value of the maximum gradually diminishes and its location shifts increasingly farther from the threshold towards larger  $p_0$ .

For a qualitative interpretation of  $\rho_\sigma$  one verifies that for the temperature  $T^* \approx 1.074m_{G0}$ , the first term of the denominator of Eq.(30) vanishes at the threshold  $p_0 = 2m_G(T^*)$ , that is Eq.(26) is equivalent to the condition for the vanishing of the first term in the denominator of Eq. (30):

$$\frac{6}{\lambda_R} - b_0^>(2m_G(T^*)) - b_T^>(2m_G(T^*)) - \frac{2}{3} \frac{\Phi^2(T^*)}{m_G^2(T^*)} = 0. \quad (31)$$

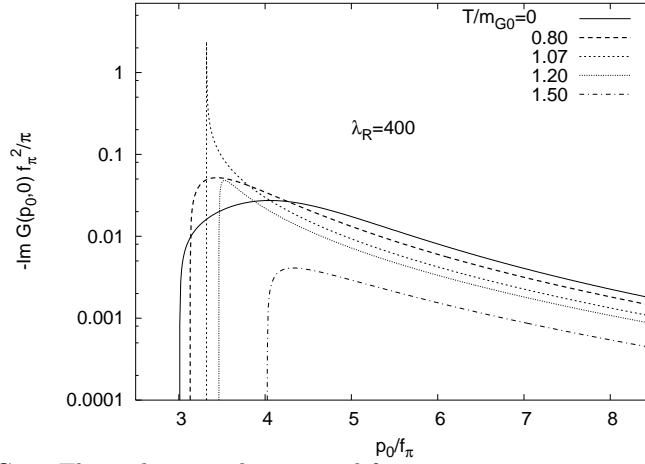


FIG. 6: The scalar-isoscalar spectral function at various temperatures

Because the term containing the real part of the bubble vanishes more rapidly at  $T^*$  as  $p_0 \rightarrow 2m_G(T^*)$  than the term containing the imaginary part of the bubble, the behavior of the spectral function around the threshold is dominated by the imaginary part of the bubble  $\rho_\sigma(p_0, 0, T^*) \sim 1/\text{Im}b^>(p_0) = 1/(1 - 4m_G^2(T^*)/p_0^2)^{1/2}$ . This is formally the same behavior exploited by Hatsuda *et al.* [3] when arguing in favor of the generic nature of the threshold enhancement phenomenon. It is worthwhile to emphasize, however, the obvious fact that according to our calculation the spectral function has nothing to do with the imaginary part of the second sheet pole which is a purely real (unphysical) quantity in this temperature regime, and the singular behavior is due to the fact that the pole along the unphysical real axis moves towards the threshold when  $T \rightarrow T^*$ .

One might suspect, that the coincidence of the pole position at  $T = T^*$  with the threshold would lead to a stronger  $\sim \delta(p_0 - 2m_G(T^*))$  singularity for this temperature. This is not true since one can easily demonstrate the vanishing of its residuum for  $T = T^*$ . The residuum of the stable  $\sigma$  pole appearing on the physical sheet for  $T > T^*$  continuously increases with the temperature.

The near threshold enhancement of the spectral function is maximal at  $T^*$ . When  $T > T^*$ , the position of the maximum moves away from the threshold and its height diminishes. This is consistent with the requirement arising from the sum rule,  $\int dp_0 p_0 \rho_\sigma(p_0) = 1$  in presence of a stable  $\sigma$ -pole with increasing residuum.

The enhancement sets in gradually and for  $T > T^{**}$  the maximum of  $\rho_\sigma$  stays very close to the actual threshold position. We can argue rather convincingly for a certain physical significance of  $T^{**}$ , when displaying  $\rho_\sigma^1(p_0) \equiv \rho_\sigma(p_0) / \sqrt{1 - 4m_G^2(T)/p_0^2}$ . The argument for this operation is the fact that the phase space volume is just proportional to the factor divided out. In Fig.7 one can follow the position of the maxima of  $\rho_\sigma$  and  $\rho_\sigma^1$  relative to the two-pion threshold as a function of the temperature. One sees that the position of  $\max(\rho_\sigma)$  touches the threshold only in a single point  $T = T^*$ . On the other hand the position of  $\max(\rho_\sigma^1(T))$  approaches  $2m_G(T)$  rather steeply, but starting from  $T = T^{**}$  the distance is found numerically always smaller than  $10^{-5}$ .

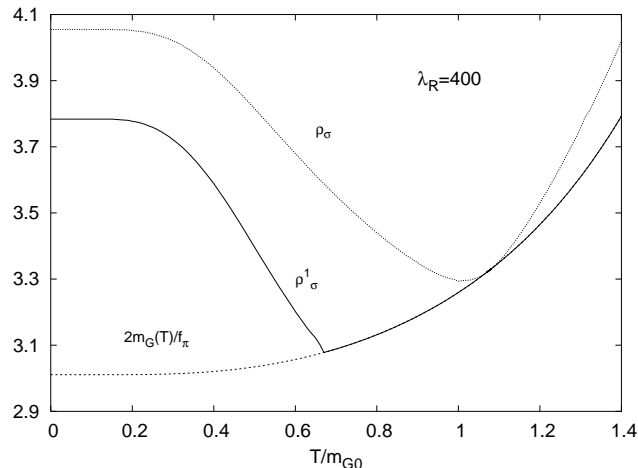


FIG. 7: The temperature dependence of the locations of the maxima of  $\rho_\sigma$  and of  $\rho_\sigma^1$  as compared to the two-pion threshold

In conclusion of this section one sees that the qualitative changes in the spectral function can be well interpreted with the help of the scalar-isoscalar pole located in the lower  $p_0$  halfplane. The threshold enhancement occurs in an extended temperature region,  $T^{**} < T < T^*$ . Any analysis attempting the reconstruction of the in-medium  $\sigma$  resonance from some experiment is necessarily based on the behavior of the scalar-isoscalar spectral function. From the above discussion it is suggestive that by the enhanced signal coming from the neighborhood of the threshold one would be led to the conclusion that in the temperature range  $T^{**} < T < T^*$  the “ $\sigma$ ” moves together with the two-pion threshold. But no trace of any Lorentzian resonance shape can be detected in the spectral function.

## VI. CONCLUSIONS

In this paper we have presented all the technical details of analyzing the pole trajectory of the propagator describing the fluctuations of the chiral order parameter in the linear sigma model with the help of a leading large  $N$  approximation. It is worth noting that the propagator of the composite field  $(\phi^a(\mathbf{x}, t))^2$  has the same poles as that of  $\phi$  in the broken symmetry phase (see Ref.[10] and references therein). Detailed mapping of the trajectory under the variation of the temperature/baryonic density as well as the parameter controlling the explicit breaking of the chiral symmetry leads us to conjecture that generically the real part of the complex pole will decrease below the two-pion threshold energy with a finite imaginary part. The application of higher order corrections in the large  $N$  expansion are expected to give no more than 25% correction. Therefore only quantitative change may happen in the scenario presented in our paper.

Our main result is the prediction that in a whole temperature range  $T^{**} < T < T^*$  the maximum of the spectral function is rather close to the actual location of the two-pion threshold. In this sense one can speak about an interval of threshold enhancement. The point of maximal enhancement is  $T = T^*$ .

The usual connection between the second Riemann sheet pole and the spectral function is restricted to the temperature range  $T < T^{**}$ . In this region the spectral function has an approximately Lorentzian shape, its maximum is centered nearly at the location of the real part of the pole, its width scales with its imaginary part. When approaching  $T^{**}$  from below, the approximately Lorentzian shape of the spectral function will be distorted, in particular it is losing its symmetry. With considerable compromise one can extend the  $\sigma$ -particle interpretation of the second Riemann sheet pole up to  $T^{**}$ .

The complete loss of this characteristic means that no resonance interpretation can be given to the pole in the  $T^{**} < T < T^*$  range. On the other hand any phenomenological analysis of a particle signal proportional to the spectral function will be peaked near the two-pion threshold in the above temperature interval. The real-time propagator in this channel will be dominated by the contribution of frequencies slightly above  $2m_G(T)$ . In this sense an increasingly narrow  $\sigma$ -signal can be detected at  $\omega \approx 2m_G(T)$  in the final two-pion spectra.

Above  $T^*$  it is a stable physical  $\sigma$ -particle, which reappears. Accordingly, the peak of the spectral function diminishes. By the increased effect of the phase space factor its maximum will be reached again at frequencies farther above the two-pion threshold.

### Acknowledgments

This research has been supported by the research contract OTKA-T037689 of the Hungarian Research Fund.

- 
- [1] T. Hatsuda and T. Kunihiro, The  $\sigma$ -meson and  $\pi - \pi$  correlation in hot/dense medium: soft modes for chiral transition in QCD, nucl-th/0112027
  - [2] S. Chiku and T. Hatsuda, Phys. Rev. **D58** (1998) 076001
  - [3] T. Hatsuda, T. Kunihiro and H. Shimizu, Phys. Rev. Lett. **82** (1999) 2840
  - [4] D. Jido, T. Hatsuda and T. Kunihiro, Phys. Rev. **D63** (2001) 011901
  - [5] K. Yokokawa, T. Hatsuda, A. Hayashigaki and T. Kunihiro, Phys. Rev. **C66** (2002) 022201(R)
  - [6] Y. Nakahara, M. Asakawa and T. Hatsuda, Phys. Rev. **D60** (1999) 091503
  - [7] F. Karsch, E. Laermann, P. Petreczky, S. Stickan and I. Wetzorke, Phys. Lett. **B530** (2002) 147
  - [8] L. Sasvári and P. Szépfalusy, J. Phys. **C7** (1974) 1061
  - [9] L. Sasvári, F. Schwabl and P. Szépfalusy, Physica **81A** (1975) 108
  - [10] A. Patkós, Zs. Szép and P. Szépfalusy, Phys. Lett. **B 537** (2002) 77
  - [11] R. S. Chivukula and M. Golden, Nucl. Phys. **B372** (1992) 44
  - [12] A. Dobado and J. Morales, Phys. Rev. **D52** (1995) 2878
  - [13] V. V. Anisovich and V. A. Nikonov, Eur. Phys. J. **A8** (2000) 401
  - [14] F. Cooper, S. Habib, Y. Kluger, E. Mottola, J.P. Paz and P.R. Anderson, Phys. Rev. **D50** (1994) 2848
  - [15] F. Cooper, S.Habib, Y. Kluger and E. Mottola, Phys. Rev. **55** (1997) 6471
  - [16] D. Boyanovsky, H.J. de Vega, R. Holman and J. Salgado, Phys. Rev. **D59** (1999) 125009
  - [17] F.E. Close and N.A. Törnqvist, Scalar mesons above and below 1 GeV, hep-ph/0204205
  - [18] N.A. Törnqvist, in Proc. of IPN Orsay workshop “Chiral fluctuations in hadronic matter”, Eds. Z. Aouissat *et al.*, p. 267, hep-ph/0201171
  - [19] A. Dobado, A. Gomez Nicola, F.J. Llanes-Estrada, J. R. Pelaez, Phys. Rev. **C66**, 055201 (2002)
  - [20] R. Brockmann and W. Weise, Phys. Lett. **B367** (1996) 40